23

Interfacial Mass Transfer and Morphological Instability of Oxide Crystal Growth

Xiuhong Pan, Weiqing Jin and Yan Liu
State Key Laboratory of High Performance Ceramics and Superfine Microstructure, Shanghai Institute of Ceramics, Chinese Academy of Sciences, Shanghai 200050, China

1. Introduction

Mass transfer near the solid-liquid interface is a fundamental problem in crystal growth and it is also a prerequisite for producing high-quality homogeneous crystals. It is desired that the mass transport phenomenon in the liquid phase can be visualized simultaneously with the growing interface. Such information is very helpful for the understanding of crystal growth mechanism. But little is known about the direct connection between mass transport and interfacial morphology in oxide crystal growth, mainly because it is technically difficult to visualize interface growth with mass flow in the high-temperature environment.

In the present chapter of the book, we take high-temperature melt (or solution) growth of oxide crystal as an example, to study the interfacial mass transport and its effect on the interfacial morphology. Most of the results are based on the experiments performed in a high-temperature in situ observation system developed by the authors (W. Q. Jin, et al., 1993), which will be firstly introduced in the following. This system is designed specially for visualizing and recording the mass transport as well as the growth process under the condition of high temperature. After that we will show the typical buoyancy and Marangoni convections in-situ observed in high temperature oxide melt in a loop-like heater. The effect of convection on the thickness of interfacial boundary layer will also be demonstrated. Then, we will discuss the diffusion-induced microconvection near the solid-liquid interface and the mass transport in the boundary layer.

The next section is devoted to deriving the correlation between the mass transfer and the interfacial morphology. After that, we shall see how external forces, such as magnetic field and mechanical vibration, stabilize the unsteady convection. Coupled with the help of external forces, effect of mass transfer near solid-liquid interface is optimized and then bulk oxide crystals with high quality are obtained by vertical zone-melting technique or vertical Bridgman growth technique. Finally, we will give a short summary and express our acknowledgments.

2. High-temperature in situ observation system

Crystal growth is a dynamic process which is composed of the mass and heat transport and interface kinetics. In this part, a high temperature in situ observation method coupling differential interference microscope and the Schlieren techniques will be introduced. The

kinetic and morphological behaviour of the growing crystals can be observed by the differential interference microscope, and Schlieren technique is applied here to visualize simultaneously convective flow in the liquid phase. Melting and growing of oxide crystal taking place in high temperature up to 1400 °C can be observed and recorded by this system.

Fig. 1 shows the photograph of the in situ observation system. The system consists of a crystal growth part, a differential interference microscope coupling with Schlieren system, and the controlling part.

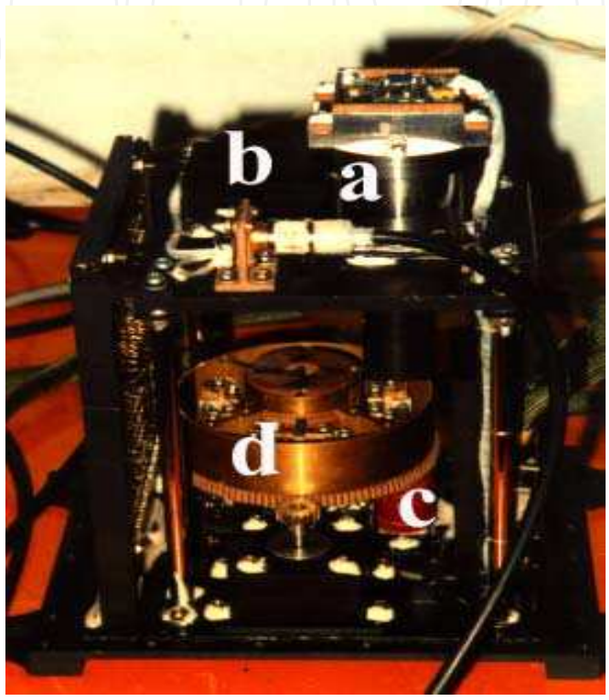

Fig. 1. The photograph of the optical in situ observation system. a: differential interference microscope coupling with Schlieren system; b: crystal growth part; c: optical light source; d: mechanical controlling part

The crystal growth part consists of a growth cell, a digital volt meter and a stabilized DC power supply. Fig. 2 shows the photo of the micro-floating-zone growth cell. A loop-like Pt wire (ϕ0.2-0.5 mm) is employed to heat and suspend the oxide melt/solution. The temperature of the loop is measured by a Pt-10%Rh thermocouple (ϕ0.08 mm). Temperature fluctuations of less than ±1 °C are obtained for high temperature melts. Two V-typed electrodes are used to prevent the loop from deformation at high temperature. For crystal growth experiment, oxide material is firstly heated and suspended horizontally on the loop heater to form a melt/solution film. The amount of the melt should be precisely adjusted so that the upper and lower planes of the thin film of the liquid are parallel to each other. Moreover, to avoid the contamination of the volatile materials, the top window in the growth cell should be eccentrically placed and rotatable. Then nucleation and crystal growth in two-dimensions are performed by decreasing the temperature of the loop heater.

A differential interference microscope is applied to visualize the crystal growth processes from the melt/solution. Schlieren technique is coupled into the microscrope for visualization

of mass flow. Fig. 3 shows the schematic of the Schlieren optical system includes two lens. The fore lens L_1 is used to form parallel rays, and a knife edge is placed at the rear focal point of lens L_2. Similarly, these parallel lights are also used to pass through the objective of the optical system of differential interference microscope. If a knife edge is installed at the rear focal point of the objective of the microscope, part of the light which has passed through the ununiform region of the object will be refracted and shielded, and the Schlieren effect can be obtained, i.e., the mass flow can be observed. So with this method, the growth pattern and the mass transportation phenomenon can be visualized simultaneously. The video from the microscope (through CCD) is recorded and visualized by the monitor. The video signal can also be transferred digitally into a computer directly for further analysis.

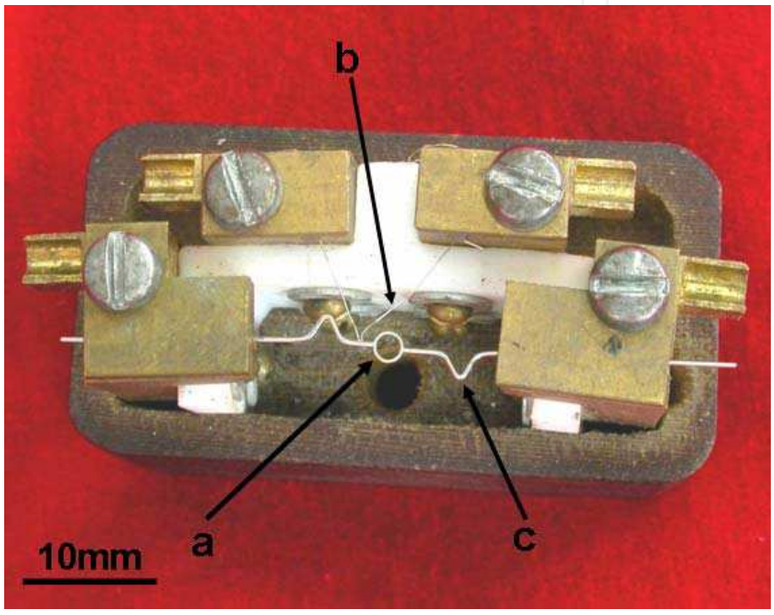

Fig. 2. The photograph of the crystal growth cell. a: loop-shaped Pt wire heater; b: Pt-10%Rh thermocouple; c: V-typed electrode

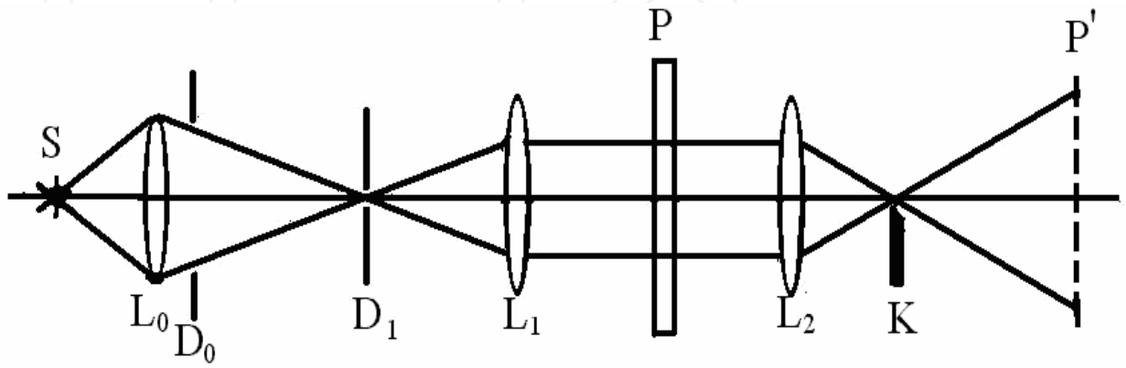

Fig. 3. Schematic figure of the Schlieren optical system. S: light source; L_0, L_1, L_2: lens; D_0,D_1: diaphragms; P: specimen; K: knife edge; P': image of P

3. Buoyancy and Marangoni convection in oxide melt

Buoyancy and thermal capillary convections (namely Marangoni convection) are the main styles of mass transfer in melt especially for high temperature condition. In this section, the typical steady buoyancy and Marangoni convections in the oxide melt/solution suspended on the loop heater will be shown. The unsteady convective flows will be illustrated in the section 6 of this chapter.

3.1 Buoyancy driven convection

Generally, buoyancy driven convection is in close correlation to the temperature distribution in the liquid phase. Fig. 4 shows the typical temperature distribution in the horizontal direction of the thin liquid film suspended by Pt loop. In the central portion of the loop, the melt temperature gradient can be negligible. This region is called pure diffusion region as indicated by sign A in Fig. 4. The situation has an advantage for studying interfacial kinetics process with pure diffusion transport. But in the marginal portion of the heater, the horizontal thermal gradient is significant, and this portion is called diffusion-convective region as hinted by the sign B in Fig. 4. In this region, the growth may be controlled by the buoyancy driven convection due to the higher temperature gradient. The width of diffusion-convective region depends on the loop diameter as well as on the thermophysical parameters of oxide melt, such as the density, thermal diffusivity and viscosity.

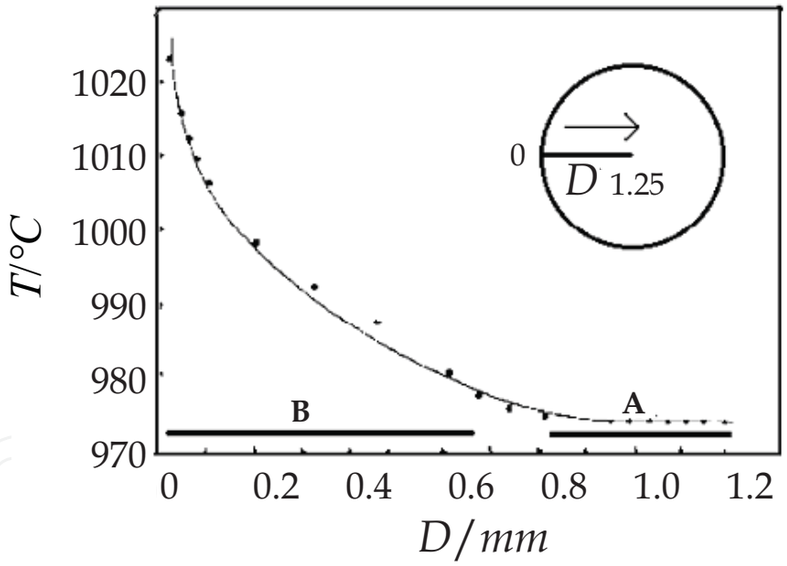

Fig. 4. Typical radial temperature distribution in the horizontal direction of the thin liquid film suspended by Pt loop. D is the distance from the loop margin. Here the temperature distribution profile is supplied for $KNbO_3$ melt

Buoyancy driven convection can be visualized since Schlieren technique has been introduced. However, quantitative measurement of flow velocity needs the help of some tracing particles. Since some tiny crystals can be nucleated when the melt becomes undercooled, the buoyancy driven convection can be indicated by observing the movement of tiny crystals as described in the reference (W. Q. Jin, et al., 1993). As shown in Fig. 5, the tiny crystals move from the margin to the center of the heater. This is typical buoyancy

driven flow caused by the melt rising along the hot wall and descending in the center of vessel which is heated from the side and cooled from the top surface. Fluid flow velocity measurement shows that the momentum profile in the melt is similar to the thermal one. In the central portion of the loop, the flow is steady because of low value of the applied temperature gradient.

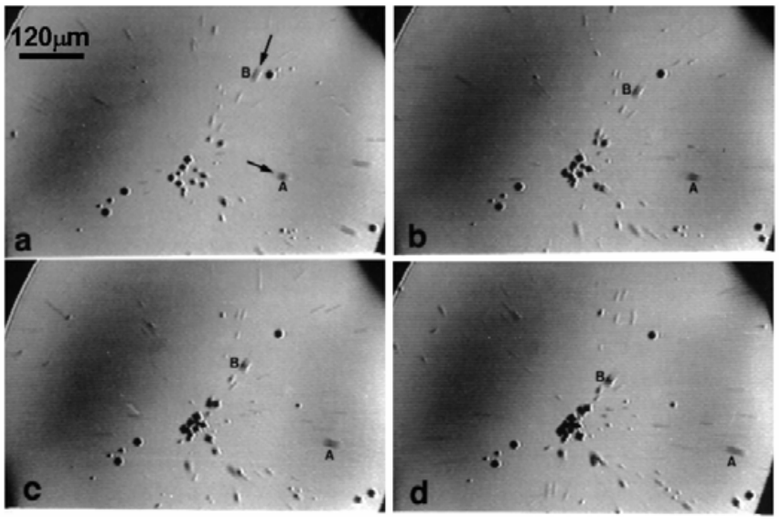

Fig. 5. The buoyancy driven convection indicated by the movement of tiny $KNbO_3$ crystals

3.2 Marangoni convection

Marangoni convection is driven by the variation of surface tension along the free surface. The temperature distribution along the azimuthal coordinate of the loop-like heater is measured by our developed non-contact method (X. A. Liang et al., 2000), which is based on the fact that dissolvability is one-valued function of the temperature. The result is shown in Fig. 6. Here $\Delta T_x=T_B-T_A$. Clearly, the temperature along the free surface is not uniform, which is caused by existence of thermocouple and other attachment. The side with thermocouple on has a lower temperature.

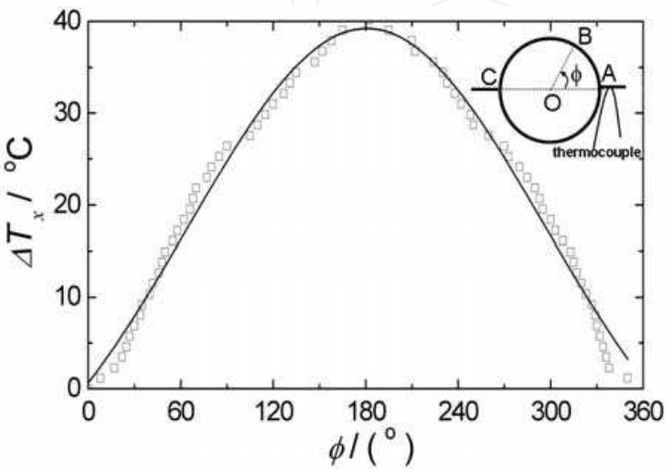

Fig. 6. Temperature difference along the azimuthal coordinate of the heater

Fig. 7 shows the streamlines of the steady Marangoni convection in the BaB_2O_4- $Li_2B_4O_7$ melt-solution. Compared with the buoyancy driven flow in the oxide melt (Fig.5), the type of Marangoni streamlines is quite different. The streamlines in Fig. 7 are concentrated at the surface. This is observed by changing the focus plane of the object lens. As one can see, the flow structure of Marangoni convection is of two symmetrical vortices, with one in the one half of the loop and its mirror image in the other half. The flow direction is from the hot point C to the cooler point A as shown in the inset of Fig.6. This is a typical pattern for Marangoni flow induced by surface tension driven convection. Such convective pattern has also been observed in $KNbO_3$ melt film (W. Q. Jin et al., 1999). It should be mentioned that if the temperature difference between the hot point C and the cooler point A exceeds some critical value, the Marangoni convection may become unsteady, which has been proved in our previous work (Y. Hong et al., 2004, 2005). Those cases are always undesired in crystal growth because growth rate fluctuation as well as microscopic defects may occur, and consequently the quality of the as-grown crystal is deteriorated.

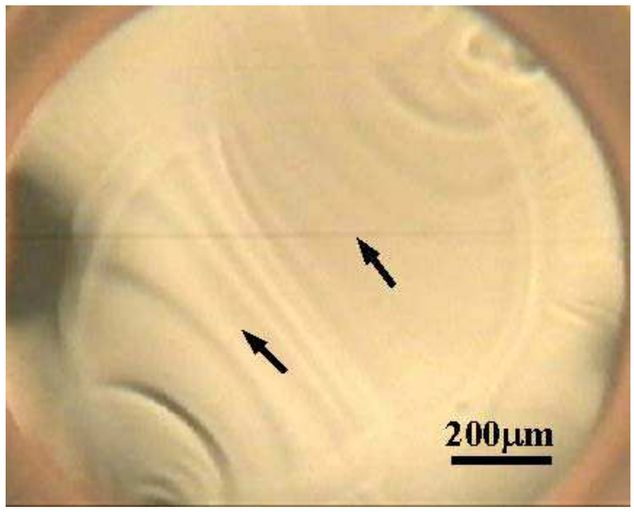

Fig. 7. Steady Marangoni convection in the BaB_2O_4- $Li_2B_4O_7$ melt-solution. The arrows indicate the flow direction

3.3 Coupling of buoyancy and Marangoni convection

The relation between buoyancy and surface tension convection is investigated in the convective region of the loop melt, since only within this region both convections exist simultaneously. In this region, a typical helix flow can be observed as shown in Fig. 8(a) and its schematic figure is drawn in Fig. 8(b). The velocities of the flow are divided into the cross section through the diameter of the loop heater (V_d) and azimuthal direction along the loop heater (V_θ), as shown in Fig. 8(c).

The flow velocity V_θ along the azimuthal direction of the loop due to the surface tension effect may be estimated by balancing the surface tension force with viscous force (F. Ai et al., 2009). This gives

$$V_\theta = C\Delta T\left(\frac{\sigma}{T} - C_\sigma\right)\exp\left(-\frac{b}{RT}\right) \tag{1}$$

where C is a geometry-dependent factor, σ is the surface tension,C_σ is specific heat at constant surface tension, b is a constant independent of temperature, and R is the gas constant.

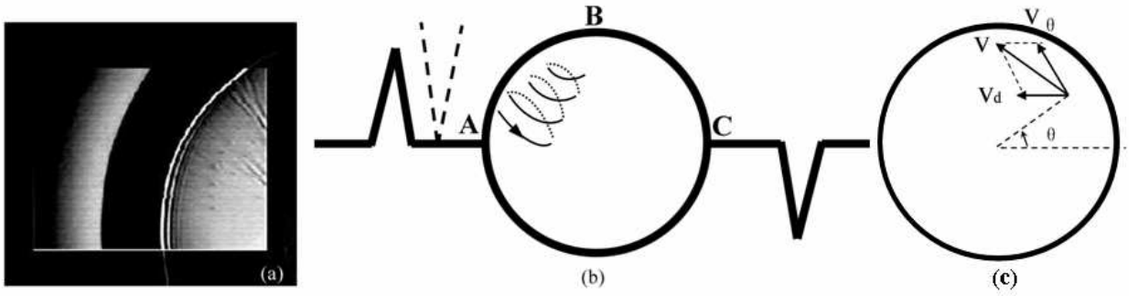

Fig. 8. Helix flow in the loop (a), the corresponding schematic figure (b) and schematic figure of the coordinates (c)

For oxide melt, by using typical values such as σ ~ 0.2 g/s² , C_σ = 1.73×10⁹ g·cm/s²·K and the experimental data, the constants can be determined as C = 2.5×10⁻⁵ cm·s/g and b/R = 1/K. Thus, from the temperature data measured, one can get the theoretical velocity along the azimuthal loop direction ($V_{s\theta}$) profile as shown in Fig. 9(a), which agrees with the experimental data ($V_{e\theta}$). This means that the flow along the azimuthal loop is mainly driven by Marangoni convection.

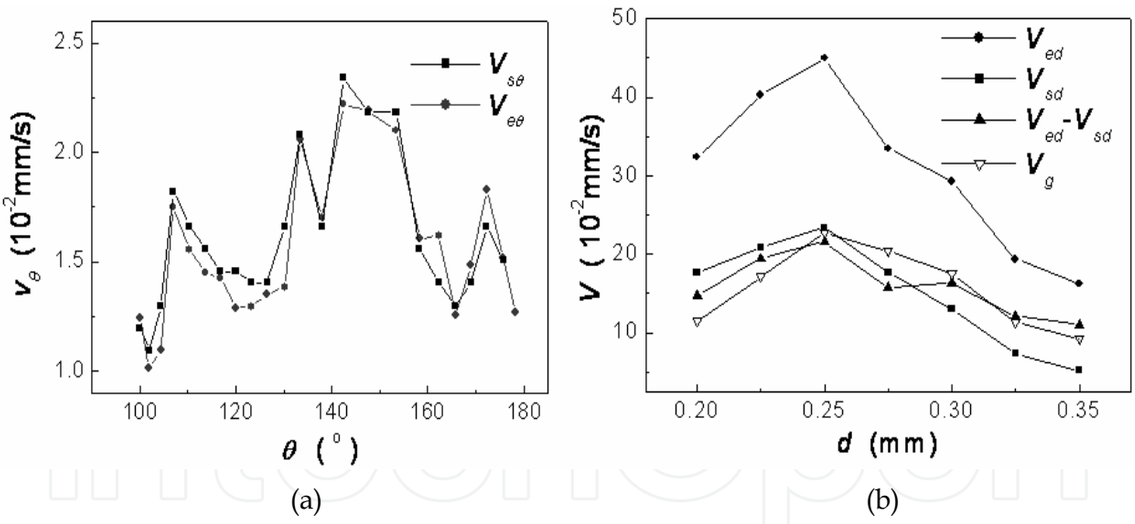

Fig. 9. (a) Comparison between experimental data $V_{e\theta}$ and theoretical calculation $V_{s\theta}$ of surface tension convection along the azimuthal direction of the loop-shaped heater; (b) The velocities of buoyancy and surface tension convection along the radial direction of the loop-shaped heater (• V_{ed} , ■ V_{sd} , ▲ (V_{ed}-V_{sd}) , ∇ V_g)

By the similar calculation process mentioned above, the convection velocity V_d, which results from the temperature difference along radial direction, can be calculated and profiled in Fig. 9(b). It is obvious that the calculated surface tension flow velocity V_{sd} is less than V_{ed} obtained by experimental data. Based on an axial symmetry solution of Navier-Stokes equation, the flow velocity V_g that is driven by buoyancy convection has also theoretically

calculated and is also illustrated in Fig. 9(b). For comparison, the profile of (V_{ed}-V_{sd}) is simultaneously illustrated. Obviously, V_g agrees well with the profile of (V_{ed}-V_{sd}). That is, the difference between V_{ed} and V_{sd} indeed results from buoyancy convection effect in present system.

4. Interfacial boundary layer and microconvection during oxide crystal growth

In crystal growth, interfacial gradients in velocity, concentration or temperature are often summarily referred to as boundary layers. The concept of interfacial boundary layer concerning of crystal growth has been thoroughly expounded by Franz Rosenberger (F. Rosenberger, 1993). The domain of liquid can be subdivided into two regions. Inside the boundary layer, the gradient is high, while out side the boundary layer, the gradient is negligible.

4.1 Calculation of interfacial boundary layer thickness

One important and effective method for calculation of interfacial boundary layer thickness is developed by the help of crystal rotation. In present high temperature in situ observation system, the rotating growth of oxide crystal has been realized (W. Q. Jin et al., 1998; X. H. Pan et al., 2008). Fig. 10 shows a typical process of BaB_2O_4 crystal growth with rotation in the center of one toroidal Marangoni flow as depicted in Fig. 7. During the growth, the Marangoni flow may be as a forced convection to rotate the tiny crystal.

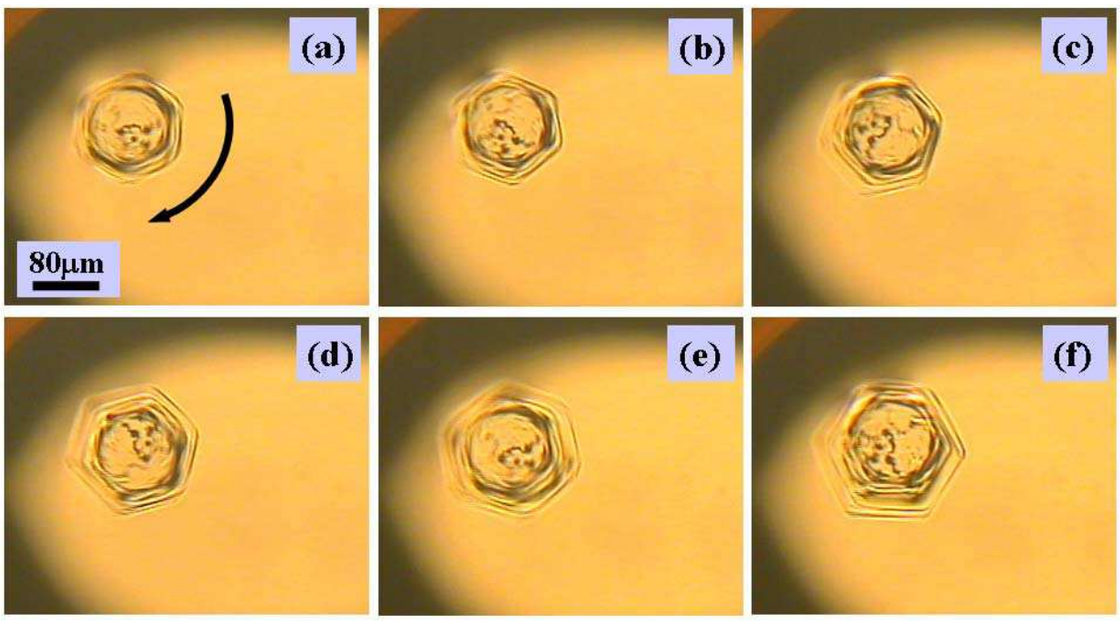

Fig. 10. BaB_2O_4 single crystal growth process with rotation. The dark arrow shows the direction of rotation and rotating velocity ω is 6 rad/s

The arrow in Fig. 10(a) illustrates the rotation direction, and the angular velocity ω is 6 rad/s. The widths of the interfacial momentum, heat and concentration boundary layer are given by following equations respectively. Where ν is the kinematic viscosity, κ is the thermal

diffusivity, D is the mass diffusivity, *P* is the Prantdl number and S is the Schmidt number. With ν = 40 mm²/s , ω = 6 rad/s, and the estimation of κ = 10^{-2}cm²/s and D = 10^{-5}cm²/s for oxide melt (W. Q. Jin, 1997), one then obtain δ_υ = 9.2 mm, δ_T = 1.25 mm and δ_C = 0.12mm, respectively.

$$\delta_\upsilon = 3.6\left(\frac{\nu}{\omega}\right)^{1/2} \tag{2}$$

$$\delta_T = 1.61\left(\frac{\nu}{\omega}\right)^{1/2} P^{-1/3} = 1.61\kappa^{1/3}\nu^{1/6}\omega^{-1/2} \tag{3}$$

$$\delta_C = 1.61\left(\frac{\nu}{\omega}\right)^{1/2} S^{-1/3} = 1.61D^{1/3}\nu^{1/6}\omega^{-1/2} \tag{4}$$

Fig. 11 shows the schematic comparison among concentration, velocity and temperature distribution at solid-liquid interface of oxide crystal growth. It is obvious that there is a big difference between the diffusivities for momentum, heat and species in the solution. The magnitudes of δ_T and δ_υ are at least one order larger than that of δ_C. This indicates that the thermal and momentum transition zone extends further into the fluid than the concentration transitional region. Thus, in the concentration boundary layer, the flow velocity and conductive heat flux are reduced to relatively small values and it is obviously meaningless to discuss interfacial heat and velocity transport in oxide crystal growth.

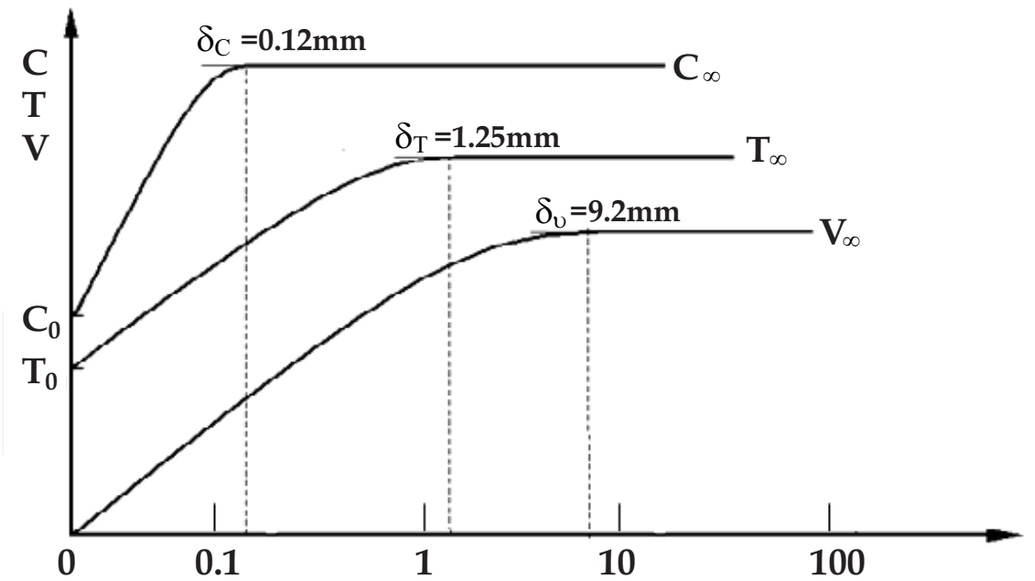

Fig. 11. Schematic comparison between δ_υ , δ_T and δ_C for BaB_2O_4 crystal rotated at 6 rad/s

One important parameter determining the thickness of interfacial boundary layer is the rotating rate ω as indicates from equations (2) to (4). Since the driving force of crystal rotation is the surface tension-driven flow caused by the horizontal temperature difference ΔT along the heater, the value of ω is consequently correlated with the strength of the Marangoni convection. Here, ΔT is the temperature difference between the hottest point C

and the coolest point A across the heater. The values of ω with various ΔT have been experimentally measured as shown in Fig. 12(a). With a larger value of ΔT, the crystal rotates faster and then a smaller width of concentration boundary layer is obtained. It should be noted that present calculating method for boundary layer thickness is unsuitable for the cases with too large or too small values of ΔT. In the former case the rotation is unsteady, while in the latter case no obvious convection is visible due to the viscous force of the melt.

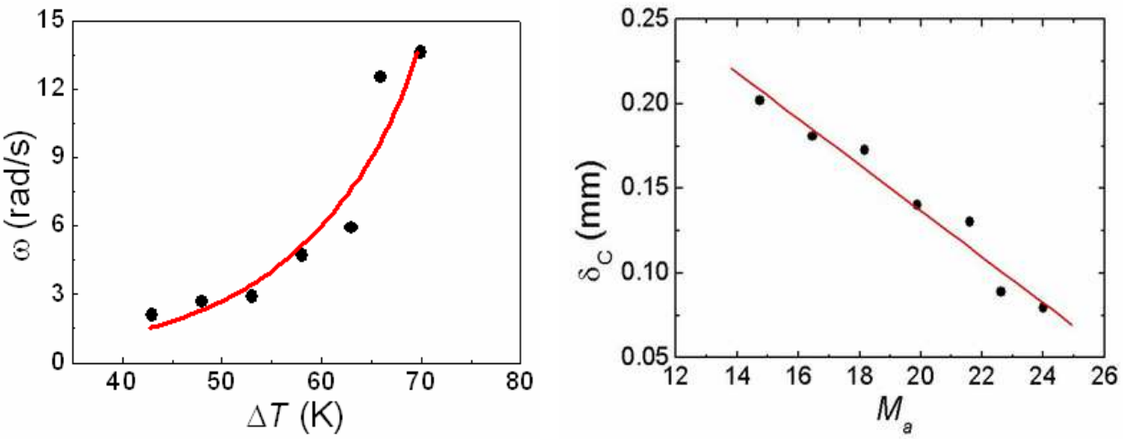

(a) (b)

Fig. 12. The dependence of rotating angular velocity on temperature (a) and the variation of concentration boundary layer thickness δ_C versus Marangoni number M_a (b)

In general, the strength of Marangoni convection can be characterized by dimensionless Marangoni number $M_a = \sigma_T \Delta T d / \eta\kappa$. Where $\sigma_T = d\sigma / dT$ is the temperature coefficient of surface tension σ, d is the characteristic length of the liquid, η is dynamic viscosity and κ is the thermal diffusivity. By taking d = 0.8 mm, σ_T = -0.06 dyn/cm•K, η = 0.16 Pa•s, and $\kappa = 10^{-2}cm^2/s$, then the calculated concentration boundary layer thickness δ_C versus M_a is plotted in Fig. 12(b). The thickness of concentration boundary layer is in inverse proportion to the value of Marangoni number. It suggests that the concentration boundary layer is suppressed by the enhancement of Marangoni convection. This is due to the fact that heat and mass transfer is enhanced and therefore the interfacial diffusion field is weakened.

4.2 Microconvection within the boundary layer

Since in the central portion of the loop, the melt/solution temperature gradient along the radial direction can be negligible, this has an advantage for studying the "pure diffusive" mass flow. Fig. 13 shows the $KNbO_3$ grains and the surrounding flow structure during growth in the center of $KNbO_3/Li_2B_4O_7$ solution. One significant flow cell is observed around each grain. Since such flow is usually restricted only in a narrow region of several tens of microns near the solid-liquid interface, that is the size scale of grain, cell or dendrite, it can be called the microconvection as described by Sahm and Tensi (P. R. Sahm and H. M. Tensi, 1981).

The growth of the grains is restricted to each other. As a result, the growing rate of the grains is much low which is helpful for velocity measurement of microconvection. The

velocity of mass flow parallel to the solid-liquid interface (transversal flow) and that of flow perpendicular to the interface (normal flow) are depicted as the solid lines in Fig. 14. Here, the origin of coordinate axes is at the center of $KNbO_3$ grain face as indicated in Fig. 13. Since the growth of the grains is restricted to each other, the quenched solution retains their situation in high temperature. And thus the solute concentration near the grain can be examined microscopically by the electron-microprobe analyses.

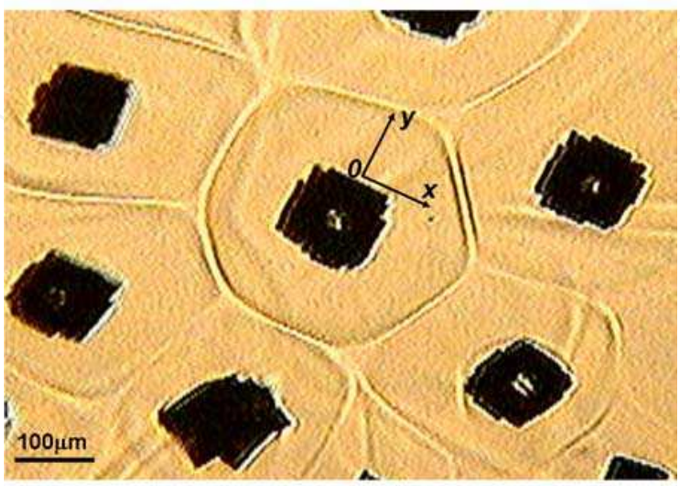

Fig. 13. Growth pattern of $KNbO_3$ solute grains in $KNbO_3/Li_2B_4O_7$ solution, showing the existence of microconvection near the solid-liquid interface

In the absence of temperature gradient for a binary system in the solution growth, it is rational to assume that the solvent is quantitatively rejected at the interface and the velocity of solvent flow is zero (W. Q. Jin et al., 2005, 2006). Then the mass transport is mainly by diffusive flux. Diffusion is in general understood as the component flux with respect to an average velocity of the system. The total mass flux of solute $KNbO_3$ in the binary system can be expressed as

$$n_K = \rho_K \upsilon_K = \rho_K \upsilon + \rho D \nabla W_K \tag{5}$$

where ρ_K is component mass density of the $KNbO_3$ solute, ρ is the total mass density, D is binary diffusivity, $W_K=\rho_K/\rho$ is the mass fraction of component $KNbO_3$, and υ is the mass average velocity

$$\upsilon = \frac{1}{\rho}\sum \rho_i \upsilon_i \tag{6}$$

For the binary system in the solution growth, the solvent is quantitatively rejected at the interface and the velocity of solvent flow is zero. So one obtain

$$\upsilon \approx \rho_K \upsilon_K / \rho = W_K \upsilon_K \tag{7}$$

So the "convective" term in (5) is

$$\rho_K \upsilon = \rho_K W_K \upsilon_K = n_K W_K \tag{8}$$

The flow in (8) is the so-called diffusion-induced bulk flow as described by Franz Rosenberger (F. Rosenberger, 1983). Substitution of (8) in to (5) yields for the "purely diffusive" component mass flux towards the growing crystal

$$n_K = \frac{\rho D}{1 - W_K} \bullet \nabla W_K \tag{9}$$

rather than the widely used

$$n_K = \rho D \bullet \nabla W_K \tag{10}$$

Furthermore, substitution of $\upsilon_K = \upsilon / W_K$ into (9), one obtains

$$\upsilon = \frac{D}{1 - W_K} \bullet \nabla W_K \tag{11}$$

Then the mass average velocity of present system in two-dimensional treatment is

$$\begin{aligned} \vec{\upsilon}(x,y) &= \frac{D}{1 - W_K(x,y)} \left(\frac{\partial}{\partial x} W_K(x,y)\vec{i} + \frac{\partial}{\partial y} W_K(x,y)\vec{j} \right) \\ &\equiv \upsilon_1(x,y)\vec{i} + \upsilon_2(x,y)\vec{j} \end{aligned} \tag{12}$$

By the experimentally measured $KNbO_3$ concentration W_K along the growing interface and normal to the interface, respectively, the authors have got the calculated profiles of velocities both along and normal to the solid-liquid interface during oxide crystal growth (W. Q. Jin et al., 2006). This is indicated by the dotted line as $\upsilon_1^t(x,0)$ and $\upsilon_2^t(0,y)$ in Fig. 14, which agrees with the experimental profile data $\upsilon_1^e(x,0)$ and $\upsilon_2^e(0,y)$, respectively. It means that on segregation at the interface, the solute diffusion-induced bulk flow is exactly nonzero and can be detected experimentally.

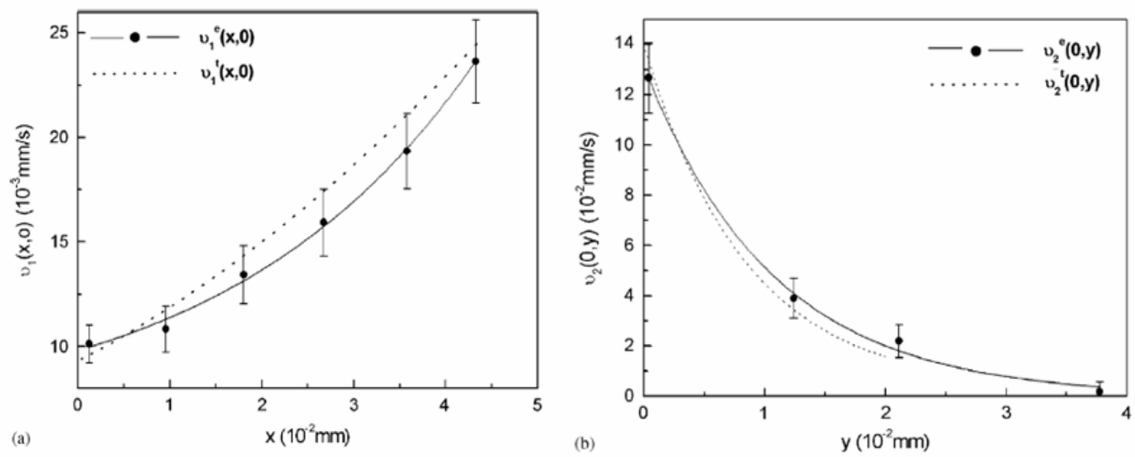

Fig. 14. Comparison between experimental velocities of $KNbO_3$ microconvection flow (solid line) and theoretical calculation velocities of $KNbO_3$ diffusion-induced bulk flow (dotted lines): (a) parallel flow to the interface $\upsilon_1(x,0)$; (b) normal flow to the interface $\upsilon_2(0,y)$

5. Effect of mass transport on interfacial kinetics and morphological instability

If only one single seed crystal is formed in the centre of the loop, it can grow larger because no surrounding grains restrain its growth. At the initial stage of growth, the crystal size is comparatively small. In this case, the growing solid-liquid interface is in the "pure" diffusion region and the interfacial mass transport visualized by Schlieren technique is shown in Fig. 15(a). However, the interfacial mass transport becomes different when the solid-liquid interface enters the diffusion-convective region near the melt margin as indicated in Fig. 15 (b). Here the mass transport is governed by the diffusive-convective flow due to the significant temperature gradient.

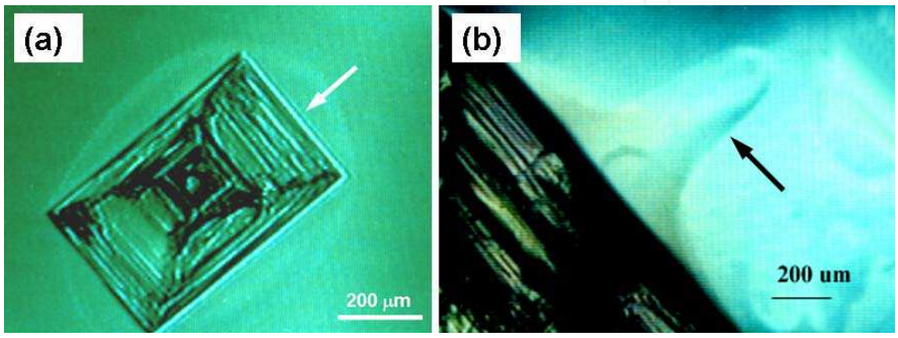

Fig. 15. Morphology of the interfacial fluid flow for one single crystal growth

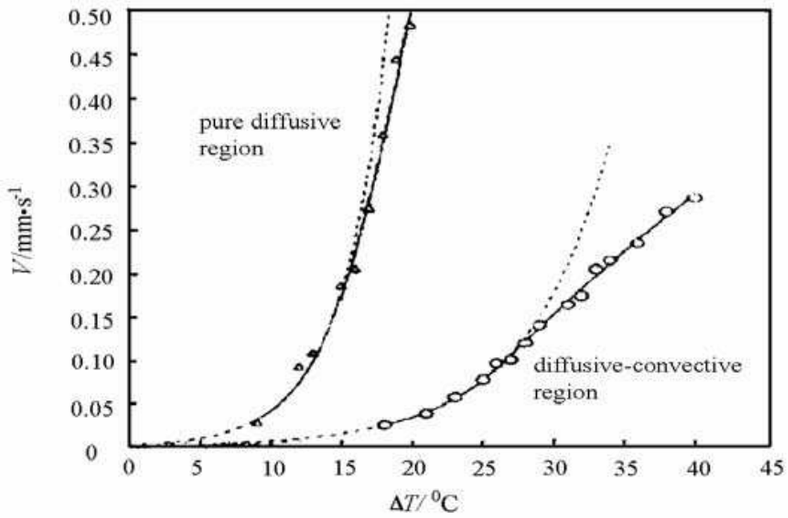

Fig. 16. The data plotted as V~ΔT for (100) face of $KNbO_3$ in the pure diffusive region and in the diffusive-convective region, respectively

To examine the influence of the mass transport on the interface growth kinetics, the growing rate data plotted as V~ΔT are shown in Fig. 16 for two different flow states. The growing rate in pure diffusive region can be described as $V=1.1\exp(-4.5\times10^4/T\Delta T)$, while that in the diffusive-convective region is expressed as $V=0.59\exp(-8.4\times10^4/T\Delta T)$. These exponential

functions indicate a growth mechanism by two-dimension nucleation. The experimental data coincide well with the dotted curves predicted by the theory of two-dimension nucleation. It can be seen that, at the lower supercoolings two-dimensional nucleation growth has been obtained irrespective of the state of mass transport in the melt. However, at the same supercooling, the discrepancy between the growth rates for two different states of convection may be assigned to the buoyancy driven convection of the interfacial mass flow.
The best model to describe the growth kinetics of two-dimensional nucleation is the birth and spread model (J. W. Cahn et al., 1964). According to this model, many nuclei occur on a flat crystal surface, and the steps annihilate when they spread and impinge. The growth rate V is given by

$$V = V_{\infty}\left(\frac{L\Delta T}{RT_m^{\,2}}\right)^{1/6} e^{\Delta G^*/3KT} \tag{13}$$

where V_{∞} is the velocity of a straight step, L is the latent heat of fusion per mole, T_m is the melting temperature, and ΔG^* is the thermodynamic potential barrier for two dimensional nucleation.
The energy barrier ΔG^* for this is given by the following equation (W. Q. Jin, 1983)

$$\Delta G^* = \frac{\pi\varepsilon^2 T_m}{L\Delta T^*} \tag{14}$$

in which ε is the free energy per unit length of a step and ΔT^* is the threshold supercooling for the growth of a flat surface. The values of ε and ΔG^* have been calculated from the experimental data for two different states of mass transport. The various results are summarized in Table.1. On comparing these experimental results with the theoretical kinetic equations (13) and (14), it is implicated that the growth kinetics is dependent upon the convection flow through the two quantities ε and V_{∞}.

mass transport state	ΔT^* (°C)	ε(J/m)	ΔG^* (J)
pure diffusive	3.0	1.2×10^{-11}	6.3×10^{-19}
diffusive-convective	5.0	1.6×10^{-11}	7.0×10^{-19}

Table 1. Data of ε and ΔG^* of $KNbO_3$ crystal growth for the (001) face in different mass transport state

The mass transport in the melt may also have great effect on the morphological stability of the growing crystal. In general, the solid-liquid interface during oxide crystal growth from high temperature melt-solution is flat and smooth for its high melting entropy, and the shape of single crystal is usually polygonal in two dimensions. However, the instability of solid-liquid interface may occur when the mass transport becomes unsteady. This is especially for the case of unsteady convection or rapid growth. Fig. 17 shows a typical unsteady growth of BaB_2O_4 melt where significant cellular shape is observed for the solid-liquid interface. Cellular growth and the resulted striations are usually found accompanied with appearance of oscillatory or turbulent flows.
In case of high cooling rate the morphology of solid-liquid interface may also become unsteady. The interfacial morphology instability has been in situ observed in the rapid

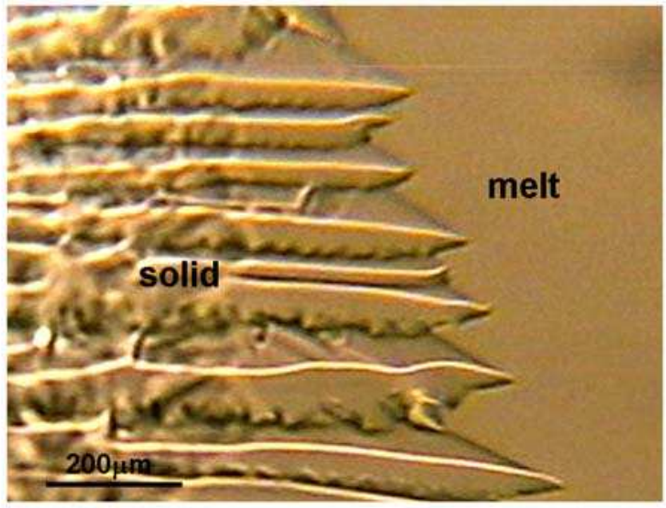

Fig. 17. Cellular interface during BaB_2O_4 crystal growth indicating the occurence of morphological instability

growth of BaB_2O_4 single crystal from high-temperature solutions (X. H. Pan et al., 2006, 2007, 2009), where skeletal shape of growing interface is obtained due to the reduction of convective regime by rapid growth. Fig. 18 shows a typical microscopic morphology of BaB_2O_4 single crystal. It is obvious that the interface is deformed and the crystal presents a shape of snowflake. This kind of interface with the centre region depressed is the so called skeletal shape. The formation of skeletal shape is the result of the extremely non-uniform supersaturation in front of the interface owing to reduction of convective effect. The concentration of solute can be examined by element detection with electro-microprobe analysis when the solution is quenched as described in section 4.2. Unfortunately, the quantitative data about interfacial concentration of BaB_2O_4 in the solution is impossible primarily due to the existence of light element boron that can not be examined effectively even by electro-microprobe technique.

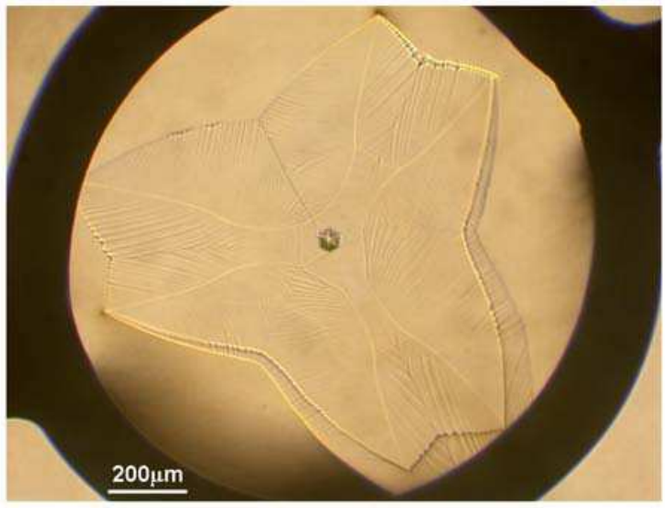

Fig. 18. Skeletal morphology of BaB_2O_4 single crystal with high growth rate

Morphological instability has also been obtained for $KNbO_3$ grains (X. H. Pan et al., 2009). Fig. 19 shows the microscopic morphologies of quenched $KNbO_3$ grains observed by electro-microprobe, which are achieved under the condition of rapid solidification. Dendrite grows in the central region of the melt indicating the appearance of morphological instability, whereas crystal with smooth surface is observed in the quenched melt adjacent to the periphery of the loop heater.

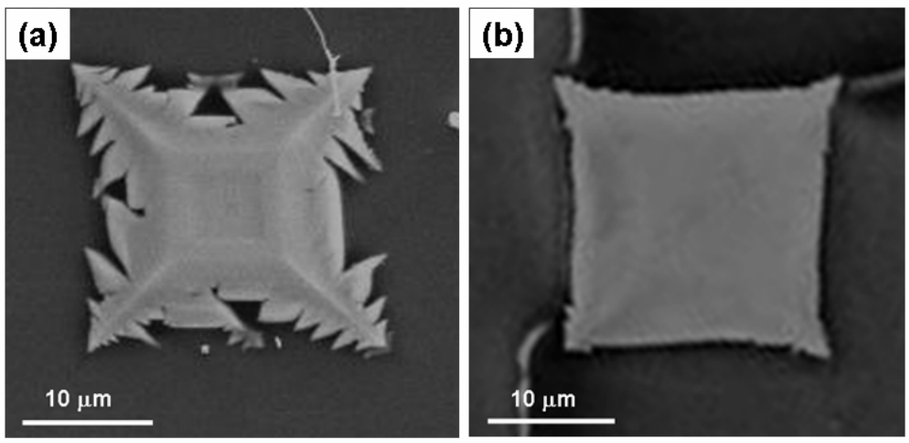

Fig. 19. Morphologies of $KNbO_3$ grains in (a) the central region and (b) the marginal region of the melt-solution observed by electron-microprobe

The instability of interfacial morphology is close by related to the solute distribution in front of the solid-liquid interface. Fig.20 shows the concentrations of solute $KNbO_3$ in the quenched melt–solution near $KNbO_3$ grains examined by electron-microprobe analysis. Here, W_{KN} is the experimentally measured mass fraction of the solute distribution in the solution and r refers to the distance in the direction parallel to the interface with origin of x-coordinate axe being at the face centre. The point "▲" is for the grain obtained in the central region while point "●" is for the grain obtained in the marginal region of the melt.

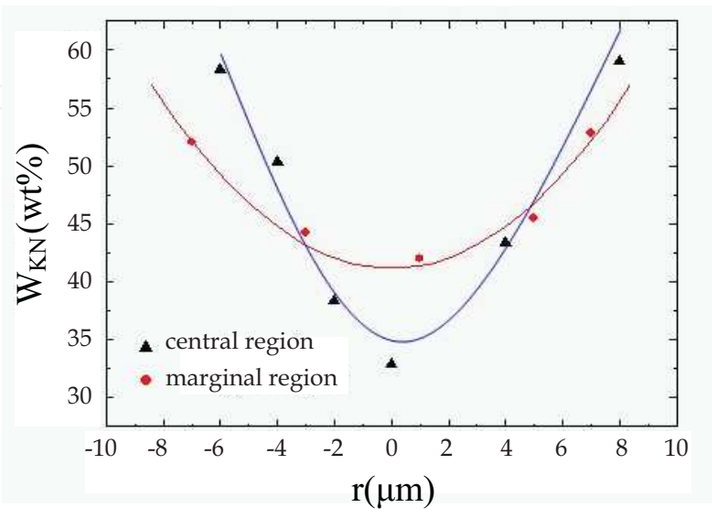

Fig. 20. Solute distribution along the solid-liquid interface of $KNbO_3$ grains in solution

It is obvious that the solute concentration along the interface is uneven both for pure diffusive and diffusive-convective regions which is in related with the specie supplies. In terms of the Berg effect, the apexes of a polyhedral crystal are the best supplied regions and the concentration along the crystal surface varies, being the lowest at the face centre. This is the shape destabilizing factor. The shape stabilizing factor is connected with the anisotropy in the surface growth kinetics. If the kinetic coefficient with its anisotropy is not sufficient to compensate for the inhomogeneity in the concentration distribution over the growing crystal face, the appearance of morphological instability in the crystal faces takes place. The curves in Fig.20 indicate that not only the concentration difference between the centre and corner of a $KNbO_3$ grain face but also the concentration gradient along the face in the convective region are lower than that in the diffusive region. This is attributed to the enhanced mass transport and thus the improved homogeneity of solute concentration by convection. As a result, morphological instability occurs more easily in the diffusive region where dendrites are found whereas crystal in the convective region conserves a polyhedral shape. This result indicates that, even underlying a very high cooling rate, flat interface may still keep its shape in case of the existence of certain convection.

It should be emphasized from above results that, only steady convection is helpful for the maintaining of flat interface during oxide crystal growth. Mass transfer governed by pure diffusion or unsteady convection may leads to morphological instability of growing interface, and thus deteriorate the crystal quality.

6. Mass transfer with external forces in oxide crystal growth

In crystal growth, steady convection is always desired because it is helpful for mass transfer and thus provides an enhanced renewal of the melt/solution in the region near the crystallization interface. However, when the temperature gradient gets larger enough, the convective flow may become oscillatory or even turbulent, which inevitably gives rise to generation of striations. In some cases, the unsteady flow may be suppressed by external force such as rotation, vibration or magnetic field. In this part, some experimental results will be given about the effect of external forces on mass transport during oxide crystal growth.

6.1 Suppression of oscillatory flow by transverse magnetic field in $NaBi(WO_4)_2$ melt

For oxide melt, oscillatory convection can be observed if the temperature gradient along the loop heater gets large enough. Fig. 21(a) shows a typical unsteady flow pattern of $NaBi(WO_4)_2$ melt. This pattern comprises one main trunk and the branches. The main trunk oscillates with time, and the arrows I, II represent the range of oscillation. Fig. 21(b) shows the schematic diagram of oscillatory pattern. The main trunk oscillates around the position A with the amplitude as shown by the bi-directional arrow 1. The oscillatory frequency reached about 10 Hz, and the amplitude was about 500 μm. Similar convective oscillations have also been observed in $KNbO_3$, BaB_2O_4 and $Bi_{12}SiO_{20}$ melts or solutions suspended on a loop heater (Z. H. Liu et al., 1998; W. Q. Jin et al., 2004; Y. Hong et al., 2006).

When a 60 mT transverse static magnetic field is applied, the distinct attenuation of the oscillation is observed and arrows III, IV represent the range of oscillation as shown in Fig. 22(a). The main trunk oscillates around the position A with the amplitude (~200 μm) as shown by the bi-directional arrow 2 in Fig. 22(b), which is smaller than that as shown by arrow 1. So the oscillatory amplitude of main trunk decreased when the magnetic field is applied. The frequency of oscillation is measured to be about 4 Hz. This means that the instability of convective flow has been effectively reduced.

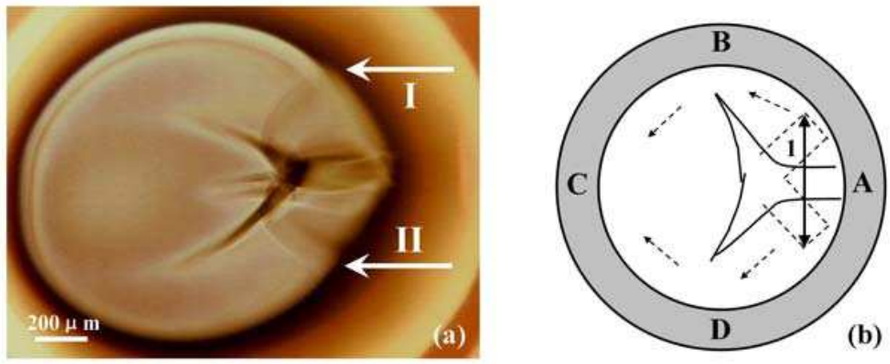

Fig. 21. (a) Oscillatory flow pattern in $NaBi(WO_4)_2$ melt, (b) The schematic diagram of the flow pattern

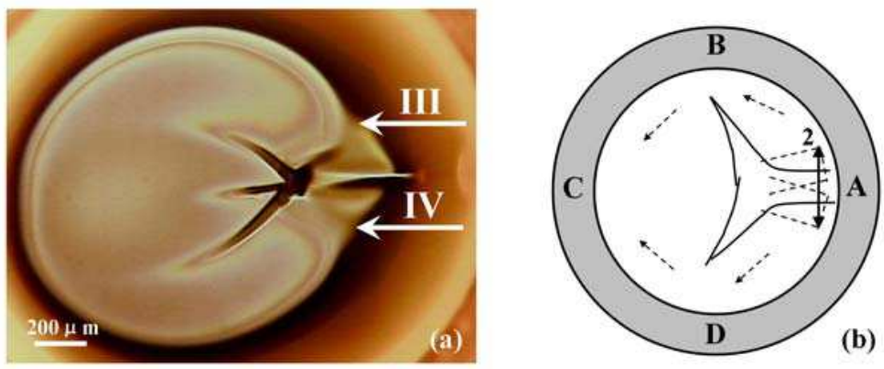

Fig. 22. (a) Flow pattern in $NaBi(WO_4)_2$ melt under 60 mT transverse magnetic field, (b) The schematic diagram of the flow pattern

In general, attention has seldom been paid to the growth of oxide single crystals in applied magnetic fields since their electrical conductivity is extremely low even in the melt. It is normally assumed that the effect of the magnetic field to be applied is negligible in an oxide melt. However, above experimental result shows that 60 mT static magnetic field is strong enough to affect the mass flow of oxide melt. It should be emphasized that the oscillation of the thermocapillary flow could be completely suppressed by the 60 mT magnetic field if the temperature difference applied on the loop decrease. The suppression of magnetic field on the oscillation flow might be due to the Lorentz force induced by the interaction of dissociated ions with magnetic field (W. Q. Jin, 2007).

6.2 Effect of rotating magnetic field on $Bi_{12}SiO_{20}$ crystal growth

In the following, the experiment results about bulk crystal growth by vertical zone-melting technique (VZM) in a rotation magnetic field (RMF) shall be demonstrated. Here $Bi_{12}SiO_{20}$ crystal is selected as model material due to its excellent photorefractive and electro-optical properties. More details about the RMF-VZM system is described in the reference (Y. Liu et al., 2010).

Fig. 23 shows the photographs of the $Bi_{12}SiO_{20}$ crystals grown by VZM. The crystal in Fig. 23(a) is grown with 25 mT and 50 Hz RMF and the one in Fig. 23(b) is obtained without RMF. A regular deep pattern with numerous curved lines is observed on the free surface

(upper part) of the as-grown single crystal obtained with RMF in Fig. 23(c). It is simplified as a schematic drawing in Fig. 23(d). Since such curved lines are observed only at the upper part of the as-grown crystal, they are in correlated with the free surface at the top end of the melt. By contrast with the same position of the single crystal grown in the normal condition without RMF shown in Fig. 23 (b), no similar pattern can be observed on the free surface of the same position. Therefore, it can be concluded that the appeared pattern is definitely induced by the applied RMF.

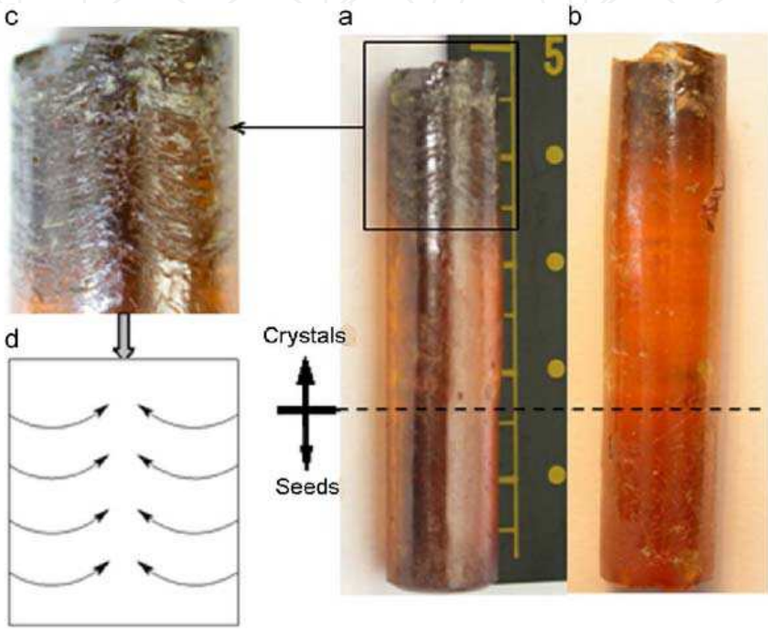

Fig. 23. $Bi_{12}SiO_{20}$ crystals grown with (a) and without (b) rotation magnetic field, the regular pattern (c) observed on the surface and its schematic drawing (d)

Optical microscopic observation reveals that the middle part of the crystal grown with RMF has no growth striations. On the other hand, a large number of growth striations could be clearly observed inside the crystal grown without RMF at the same position. This is due to the appearance of steady forced convection in the melt induced by magnetic field. As a result, the transport of heat and mass is enhanced and remains stable, and therefore the crystallographic perfection could be improved.

6.3 Improvement of crystallographic perfection in $Bi_{12}SiO_{20}$ crystal by axial vibration

The authors have experimentally investigated the effect of axial vibration on the free surface flows in a vertical Bridgman model under isothermal conditions (X. H. Pan, 2005a, 2005b). Steady forced flows are obtained on the free surface of the liquid phase driven by pure axial vibration. Based on this hinting, axial vibration is introduced into the $Bi_{12}SiO_{20}$ crystal growth in our laboratory (Y. Zhang et al., 2008, 2009), in order to suppress the unsteady thermocapillary or buoyancy convections. Some results are described in the following.

Axial vibration has been introduced in the growth of $Bi_{12}SiO_{20}$ single crystal by vertical Bridgman technique. The frequency of the axial vibration applied is 50 Hz and its amplitude varies. The quality of the $Bi_{12}SiO_{20}$ single crystal is identified by the high-resolution X-ray rocking curves as shown in Fig. 24. It can be found that the crystal grown with 70 μm

vibration has the strongest diffraction intensity and the smallest full-width at half-maximum (FWHM), indicating the highest crystal quality. This means that crystallographic perfection of oxide crystal can be effectively improved by axial vibration with proper amplitude.

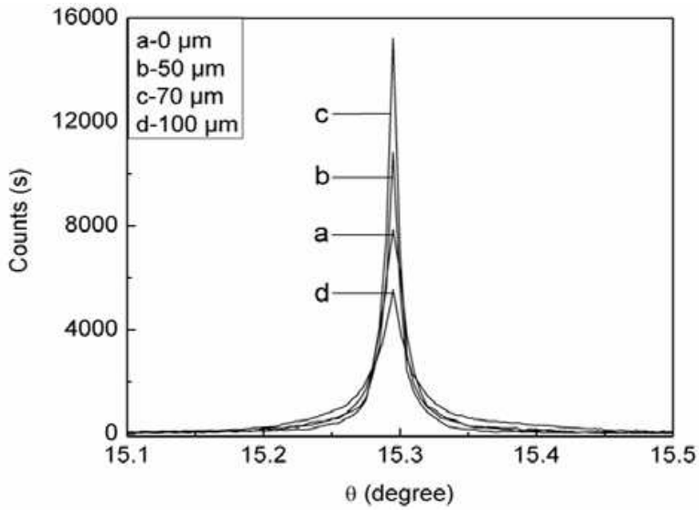

Fig. 24. X-ray rocking curves of $Bi_{12}SiO_{20}$ crystals grown by vertical Bridgman method with different vibration amplitudes

Fig. 25 shows the etch pit pattern of the as-grown $Bi_{12}SiO_{20}$ crystals by vertical Bridgman method. The etch pit density of the crystal grown without vibration is about $4.8\times10^4/cm^2$ (Fig. 25(a)). However, when an axial vibration of 70 μm amplitude is applied, the etch pit density of the crystal grown with vibration is only $2.2\times10^4/cm^2$ (Fig. 25(b)). This is attributed to the enhanced mass exchange and the diminished radial temperature gradient in front of the solid-liquid interface by vibration-induced forced convection.

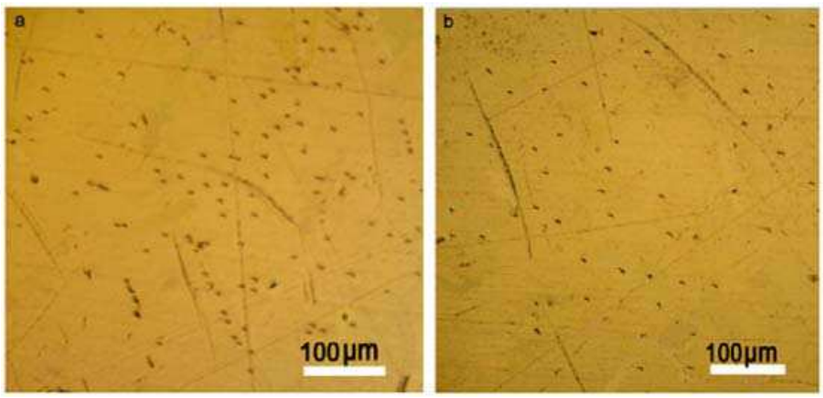

Fig. 25. Etch pit patterns of $Bi_{12}SiO_{20}$ crystals grown without vibration (a) and with vibration of 70 μm amplitude (b)

7. Summary and conclusions

The coupling of differential interference microscope and the Schlieren technique is an effective method to visualize the mass transport simultaneously with the growing interface

for oxide crystal growth. Besides the buoyancy and Marangoni convections induced by temperature gradient, diffusion-induced micro-convection in the boundary layer also exists. The style of mass transfer near the growing interface has great effect on the interfacial kinetics and the interfacial instability. The mass transport governed by pure diffusion can induce inhomogeneous concentration distribution along the growing interface of the single crystal and thus leading to morphological instability, where dendritic or skeletal shape occurs easily. Nevertheless, if the mass transport is governed by both convection and diffusion, the faceted interfacial shape is easy to maintain. The mass transport can be effectively improved by external forces such as magnetic field and vibration, and thus single crystal with high crystallographic perfection can be obtained.

8. Acknowledgements

The authors would like to thank their colleagues and collaborators. The author would also like to acknowledge the supports from National Natural Science Foundation of China under Grant Nos 50802105 and 50331040.

9. References

F. Rosenberger, (1983). Interfacial transport in crystal growth, a parametric comparison of convective effects. *Journal of Crystal Growth*, Vol.65, pp. 91-104

F. Rosenberger,(1993). Boundary layers in crystal growth-facts and fancy. *Progress in Crystal Growth and Material Characterization*, Vol.26, pp.87-98

F. Ai, W. Q. Jin, H. S. Luo, Y. Liu & X. H. Pan, (2009). Study on the buoyancy and surface tension convection of high-temperature oxide solution. *Materials Chemistry and Phsyics*, Vol.114, pp. 387-390

J. W. Cahn, W. S. Hilling & G. W. Sears (1964). The molecular mechanism of solidification. *Acta Metallurgica*, Vol.12, pp.1421-1439

P. R. Sahm & H. M. Tensi, (1981). Mass transport in the near vicinity of solidification fronts under microgravity. *Advances in Space Research*, Vol. 1, pp. 97-110

W. Q. Jin, (1983). Ph.D. Thesis, University of Tohoku, Sendai, Japan, P.179, in Japanese

W. Q. Jin, J. Y. Chen, W. S. Li & H. P. Yan, (1993). Development of optical system for high temperature in situ observation of oxides crystal growth. *Ferroelectrics*, Vol.142 pp.13-18

W. Q. Jin, J. Y. Chen & W. S. Li, (1993). High temperature in situ observation of the melt transfer process around growing $KNbO_3$ crystal. *Microgravity Quarterly*, Vol.3 pp.129-133

W. Q. Jin, Z. L. Pan, N. Cheng & Y. Hui, (1997). Boundary layer effect in crystal growth – comments on the optical in situ observation technique for melt crystal growth. *Journal of Inorganic Materials*, Vol. 12, pp. 279-285 (in Chinese)

W. Q. Jin, Z. L. Pan & Z. H. Liu, (1998). Effect of buoyancy-driven convection upon crystal growth of $KNbO_3$ in the melt. *Journal of Crystal Growth*, Vol. 191, pp. 760-766

W. Q. Jin, Z. L. Pan & C. Ning, (1999). Experiments on surface tension driven flow in high temperature oxide melting. *Space Forum*, Vol. 4, pp. 321-330

W.Q. Jin, X.A. Liang, Y. Hong, X.H. Pan & K. Tsukamoto, (2004). Study on thermocapillary convection in $Bi_{12}SiO_{20}$ melt. *Journal of Crystal Growth*, Vol. 271, pp. 302-306

W. Q. Jin, (2005). Diffusion effect in solidification. *Journal of Inorganic Materials*, Vol. 20, pp.42-46 (in Chinese)

W. Q. Jin, X. H. Pan, Y. Liu, Y. Hong, Y. F. Jiang & S. Yoda, (2006). Two-dimensional mass diffusion-induced bulk flow in a boundary layer of crystal growth. *Journal of Crystal Growth*, Vol. 293, pp. 198-202

W. Q. Jin, F. Ai, Y. Hong, H. S. Luo, Y. Liu & X. H. Pan, (2007). The attenuation of oscillatory thermocapillary convection in the oxide melt by a transverse magnetic field. *Science in China Series G*, Vol. 50, pp. 519-524

X. A. Liang, W. Q. Jin, Z. L. Pan & Z. H. Liu, (2000). Experimental measurement of temperature distribution across a loop-like heater. *Progress in Crystal Growth and Material Characterization*, Vol. 40, pp. 301-307

X. H. Pan &W. Q. Jin, (2005). Effect of axial vibration on free surface flows in cylindrical liquid. *Chinese Physics*, Vol. 14, pp. 422-426

X. H. Pan, (2005). Ph.D. Thesis, Shanghai Institute of Ceramics, CAS, Shanghai, China, P. 125, in Chinese

X. H. Pan, W. Q. Jin, Y. Hong & F. Ai, (2006). In situ observation of skeletal shape transition during BaB_2O_4 crystal growth in High-temperature solution. *Chinese Physics Letters*, Vol. 23, pp. 2269-2272

X. H. Pan, F. Ai, W. Q. Jin, Y. Liu & Y. Zhang, (2007). Morphologies of solid-liquid interface and surface steps during rapid growth of BaB_2O_4 single crystals. *Science in China Series G*, Vol. 50, pp. 539-545

X. H. Pan, W. Q. Jin, Y. Liu & F. Ai, (2008). Effect of surface tension-driven flow on BaB_2O_4 crystal growth from high temperature melt-solution. *Crystal Research and Technology*, Vol. 43, pp. 152-156

X. H. Pan, W. Q. Jin, Y. Liu & F. Ai, (2009). Solute distribution in $KNbO_3$ melt-solution and its effect on dendrite growth during rapid solidification. *Chinese Physics B*, Vol. 18 , pp. 699-703

Y. Hong, W. Q. Jin & X. H. Pan, (2004). Thermalcapillary convection in $NaBi(WO_4)_2$ melt. *Chinese Physics Letter*, Vol. 21, pp. 1986-1988

Y. Hong, W. Q. Jin, X. H. Pan, &Y. Shinichi,(2005). Effect of free surface deformation on thermocapillary convection in high Prandl number melt. *Journal of Crystal Growth*, Vol. 274, pp. 480-485

Y. Hong, W. Q. Jin, X. H. Pan & Y. Shinichi, (2006). Experimental study on marangoni convection and solidification in BaB_2O_4 melt. *International Journal of Heat and Mass Transfer*, Vol. 49, pp. 4254-4257

Y. Liu, Fei Aai, X. H. Pan, Y. Zhang, Y. F. Zhou & C. D. Feng, (2010). Effect of rotating magnetic field on $Bi_{12}SiO_{20}$ crystal growth by vertical zone-melting technique. *Journal of Crystal Growth*, Vol. 312, pp. 1622-1626

Y. Zhang, Y. Liu, W. Jiang, X. H. Pan, W. Q. Jin & F. Ai, (2008). Vertical Bridgman growth of $Bi_{12}SiO_{20}$ crystal with axial vibration. *Journal of Crystal Growth*, Vol. 310, pp. 5432-5436

Y. Zhang, Y. Liu, W. Jiang, X. H. Pan, W. Q. Jin, F. Ai & H. C. Wang, (2009). Effect of axial vibration on $Bi_{12}SiO_{20}$ crystal growth by Vertical Bridgman technique. *Crystal Research and Technology*, Vol. 44, pp. 248-252

Z. H. Liu, W. Q. Jin, Z. L. Pan & N. Cheng, (1998). Experiments on surface tension driven flow in high temperature oxide melt. *Journal of Inorganic Materials*, Vol. 13, pp. 113-116 (in Chinese)

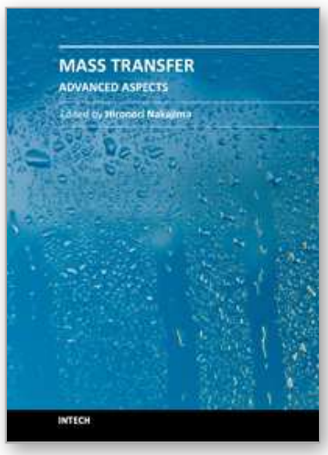

Mass Transfer - Advanced Aspects

Edited by Dr. Hironori Nakajima

ISBN 978-953-307-636-2
Hard cover, 824 pages
Publisher InTech
Published online 07, July, 2011
Published in print edition July, 2011

Our knowledge of mass transfer processes has been extended and applied to various fields of science and engineering including industrial and manufacturing processes in recent years. Since mass transfer is a primordial phenomenon, it plays a key role in the scientific researches and fields of mechanical, energy, environmental, materials, bio, and chemical engineering. In this book, energetic authors provide present advances in scientific findings and technologies, and develop new theoretical models concerning mass transfer. This book brings valuable references for researchers and engineers working in the variety of mass transfer sciences and related fields. Since the constitutive topics cover the advances in broad research areas, the topics will be mutually stimulus and informative to the researchers and engineers in different areas.

InTech Europe
University Campus STeP Ri
Slavka Krautzeka 83/A
51000 Rijeka, Croatia
Phone: +385 (51) 770 447
Fax: +385 (51) 686 166
www.intechopen.com

InTech China
Unit 405, Office Block, Hotel Equatorial Shanghai
No.65, Yan An Road (West), Shanghai, 200040, China
中国上海市延安西路65号上海国际贵都大饭店办公楼405单元
Phone: +86-21-62489820
Fax: +86-21-62489821

IntechOpen